CNN-based fish iris identification

Rudolf Schraml[1] • Georg Wimmer[1] • Heinz Hofbauer[1] • Ehsaneddin Jalilian[1] • Dinara Bekkozhayeva[2] • Petr Cisar[2] • Andreas Uhl[1]

[1]Department of Computer Sciences, Paris Lodron University of Salzburg, Austria
({rschraml,gwimmer,hofbauer,ejalilian,uhl}@cs.sbg.ac.at)
[2]Institute of Complex Systems, University of South Bohemia in České Budějovice, Czech Republic
({dbekkozhayeva,pcisar}@frov.jcu.cz)

February 23, 2023

Abstract

As in many other areas, digitization is also on the rise in intensive aquaculture. A vision for the future is continuous monitoring and the recognition of each individual fish in the system. Previous work has shown that Atlantic salmon can be recognized using lateral and iris images. For salmon iris identification a traditional texture feature-based approach was used. Results indicated a high distinctiveness but a low stability of the salmon iris. In this work we employ a CNN-based fish iris identification approach and reassess the previous results. One question is whether a CNN-based approach performs better in terms of long-term stability. Furthermore, a second database for European seabass iris images is used in the experiments. This makes it possible to check the applicability of iris identification in another fish species and whether the statements regarding distinctiveness and stability are also confirmed here. Results show that the CNN-based approach performs worse compared to the texture feature-based approach. Same as for the salmon iris a high distinctiveness of the seabass iris but a low stability can be reported.

Contents

1 Introduction

The growing population as well as the increasing prosperity requires to improve food production. Intensive aquaculture is significant to be able to guarantee fish supply. However, further increases in production through a higher density of fish go hand in hand with an increasing risk of diseases in the stock. The solution is to deal with fish welfare when increasing the production which is referred to as eco-intensification. One building block to deal with fish welfare is to monitor the stock on a fish by fish basis. Continuous monitoring makes it possible to identify changes or anomalies in the fish population at an early stage and to take targeted countermeasures.

For this work, we deal with non-invasive methods. Tagging or marking is not feasible in the context of intensive aquaculture because of cost and fish welfare issues. Related research published in the aquaculture community refers to the term photo identification in case that biometric identification of aquatic individuals using images is performed. Most works target at semi-supervised identification for research where non-invasive identification is required in order to avoid adverse effects caused due to stress. Although there exists plenty of research, only a few approaches make use of machine vision methods. Even then, researchers mostly used machine vision in order to assist photo, i.e. naked eye, identification. A rough subdivision of the previous approaches can be made on the basis of the body part that was photographed. In [1, 2, 3] the authors used lateral images of various fish species for identification experiments. Furthermore, dorsal head or ventral images have been used as biometric characteristics in [4, 5] and [6], respectively. Some of these work presents promising results, however, there are two fundamental problems with all of them: (i) the region which contains the biometric information needs to located manually and (ii) it has been shown that skin patterns change over time.

Therefore, for the experiments in [7, 8] iris and lateral skin pattern images of 330 Atlantic salmon fish were captured. 30 fish were photographed three more times with an interval of two months in between. In [7] the fish iris has been utilized as biometric characteristic and, apart from image acquisition, a fully automated fish identification system has been demonstrated. The database enabled to investigate the distinctiveness and stability of the salmon fish iris. Results showed that the fish iris is highly distinctive and identification rates of over 95% could be achieved. However, the long term experiments showed a weak stability of the fish iris which needs to be considered in a biometric system. For feature extraction and matching an iris-based approach inspired by human recognition was applied, i.e. Log-Gabor filters for feature extraction and the hamming distance for matching. In [8] the authors propose a fully automated system using dorsal skin pattern images of the dataset. Images were taken for fish out of the water and in the aquarium to test real conditions. The region of interest (ROI) containing the dot pattern in each image was located automatically. The authors proposed two different approaches for feature extraction and matching. The first one, denoted as dot-based approach uses a convolutional neural network (CNN) which is trained to localize dots in the ROIs. A special algorithm was developed for comparing the dot patterns, which also compensates for shift and rotation variances. Second, Histogram of Gradients (HOG) based feature extraction was applied which enabled to utilize a distance metric for the matching procedure. Same as for the dot-based approach the HOG approach was adapted to compensate shifting in x- and y-direction. For the aquarium images the dot-based approach showed 100% identification accuracy for the short term dataset and it could be shown that up to 4 months all fish could be still correctly identified. It could be demonstrated that the dot pattern is highly distinctive and shows a higher stability compared to the fish iris.

For this work, we focus again on the fish iris for individual fish identification in order to take up and examine further questions. Thus, for feature extraction and matching a CNN-based approach is employed. CNN-based approaches outperformed traditional handcrafted feature extraction and matching approaches for various biometric characteristics in human recognition [9]. The question is whether a CNN-based approach to fish iris recognition can improve identification performance for both, the short term and the long term. Last but not least, we want to investigate whether iris recognition can also be used with another fish species. Thus, a new database was captured which enables to examine if fish iris recognition is feasible for another species and if the basic statements vary with different fish species or not. Thus, for the experiments a new database with iris images for European seabass has been captured. A CNN-based feature extraction and matching approach for fish iris recognition is employed and assessed for the new database as well as for the Atlantic salmon database.

First, in Sec. 2 the databases are introduced, followed by the description of the identification pipeline for the texture feature-based and the CNN-based approach. Subsequently, the experimental setup is presented in Sec. 3 followed by a discussion of the results in Sec. 4. Sec. 5 concludes this work.

2 Materials and Methods

First, the two databases (DBs) used are described and then the individual steps of the fish iris identification pipeline are considered in detail.

2.1 Atlantic salmon and European seabass Iris Image DBs

The first DB, denoted as Atlantic Salmon Iris Image Database (AS_{DB}) was captured from Atlantic salmon at the NOFIMA

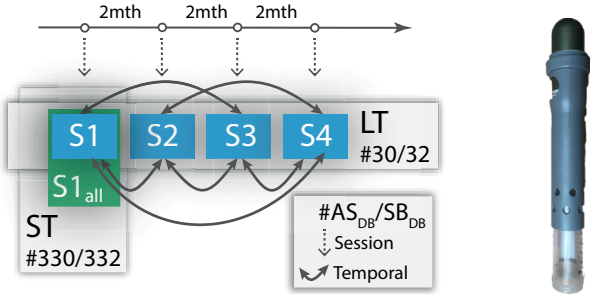

Figure 1: DB overview and USB microscope

research station in Sunndalsora, Norway. SIIDB is the same database as utilized in [7]. In this data acquisition, lateral salmon images were also taken of the same fish which were used for the experiments presented in the work by [8]. The second DB, referred to as Seabass Iris Image Database (SB_{DB}) was collected at the Hellenic Centre for Marine Research in Heraklion, Greece. Iris and lateral images were also taken of these fish. Exemplary lateral salmon and seabass images are shown in Fig. 2a and Fig.2b, respectively. For both DBs a microscope (Dino-Lite AM3113T) was utilized to capture the fish iris. In order to achieve a constant distance, the microscope was fixed to the upper end of a tube which was placed over the fish eye for the recordings (see Fig. 1).

Fish were anesthetized and one iris was captured 8–16× with the fish head showing to the left. The fish was slightly moved and rotated between shots to create variance. Unusable images were removed to avoid problems.

As illustrated in Fig. 1 AS_{DB} and SB_{DB} are subdivided into short term (ST) and a long term (LT) datasets. For AS_{DB} the ST dataset is composed of iris images from 330 salmon fish and for the SB_{DB} ST dataset iris images of 332 seabass fish were captured. For the LT datasets of AS_{DB} a subset of 30 fish of the ST dataset were pit-tagged and captured again in three subsequent sessions (S2,S3,S4) with approximately two months time span in between. The LT dataset of SB_{DB} is composed by 32 fish out of the respective LT dataset. The 32 fish were pit-tagged and captured once again after a period of two months. Exemplary iris images for both DBs are shown in Fig. 2c and Fig. 2d. Fig. 2c shows the salmon iris images of one fish of the LT dataset captured in the four sessions. In Fig. 2d the LT dataset images captured in two sessions for two different seabass fish are shown.

2.2 Identification pipeline

Subsequently, the identification pipeline as applied in the experiments is outlined.

2.2.1 Iris Localization

The first step in the pipeline is to locate the iris in an image and to segment it from the background. For the iris the inner and outer boundary, which are referred to as pupillary and limbic boundary, respectively, need to to be located. Basically, the same CNN-based semantic segmentation-based as

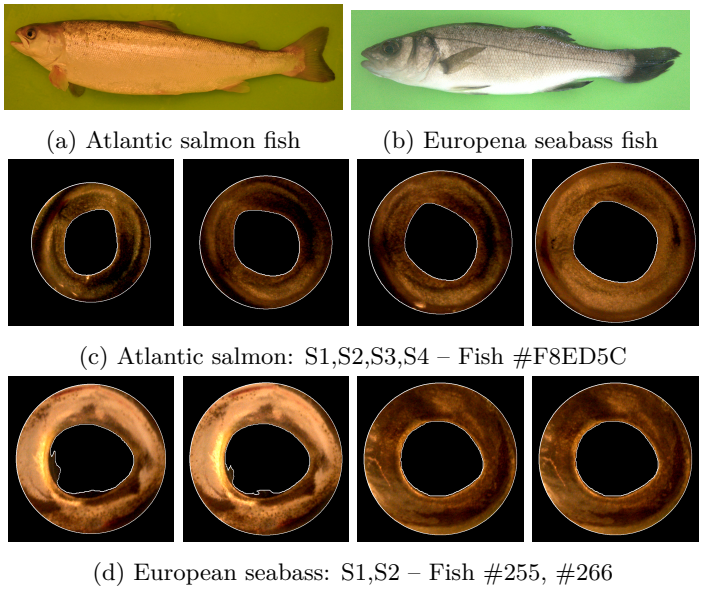

(a) Atlantic salmon fish (b) Europena seabass fish

(c) Atlantic salmon: S1,S2,S3,S4 – Fish #F8ED5C

(d) European seabass: S1,S2 – Fish #255, #266

Figure 2: Exemplary lateral Atlantic salmon and European seabass images of AS_{DB} and SB_{DB} and exemplary iris images from the LT datasets.

proposed in [7] is used. As with the salmon iris, the limbic boundary of the seabass iris could not be determined either, even not manually. Thus, the CNN is only used to separate the pupillary from the background. The pupillary groundtruth data to train a CNN for each DB is generated in a semi-automated manner (see [7]). A two-fold scheme has been applied for each DB to get the pupillary boundary for each iris image. In order to approximate the limbic boundary, the center of mass (CM) of the pupillary and the mean distance value between the CM and pupillary boundary distances are computed. The limbic boundary is then specified by a circle centered at the pupillary CM and a radius which is two times larger than the computed mean distance. Exemplary segmentation results for both DBs are shown in Fig. 2c and Fig. 2d

2.2.2 Rotational pre-alignment

Both DBs show differences in the rotation of a fish's iris. These were caused by the recording protocol, where several pictures were taken when recording an iris and the fish was moved and rotated slightly between the individual images in order to generate variances in the data. However, as shown in the iris images in Fig. 2c and Fig. 2d there is less rotation in the iris images of SB_{DB}. In order to compensate for rotational variances the PCA and MAX strategies as proposed in [7] are utilized. Both strategies were suited for the Atlantic salmon iris which is not circular and enables to determine a pre-alignment vector. The seabass iris looks similar and thus, both strategies will be applied an evaluated in this work. For principal component analysis (PCA) the perpendicular eigenvectors of the pupil are computed and the dominant axis is used as pre-alignment vector (Θ_0). In case of MAX the pupillary boundary is smoothed and the

maximum CM to pupillary boundary vector is utilized as Θ_0.

2.2.3 Texture Feature-based fish iris recognition

As in [7], feature extraction & matching are performed similar to classical human iris biometrics. For this purpose, the iris is polar transformed and normalized using Daugman's rubber-sheet model [10]. The rotational pre-alignment vector Θ_0 is used as initial vector to unroll the iris into the polar domain. For feature extraction the 1-D-Log-Gabor [11] based feature extraction approach from the open University of Salzburg Iris Toolkit (USIT) [12] is used. The calculated feature vectors are compared with one another using the Hamming distance. For more details we refer to [7].

CNN-based fish iris recognition Deep-learning based methods were tested in the field of human biometrics for most biometric characteristics now [9]. This is also the case in iris recognition (e.g. in [13]), where CNN-based methods were able to show significant improvements in regard to the identification performances compared to traditional texture feature-based methods. For this reason, in this work a CNN-based approach using the triplet loss function [14] is employed. For biometric applications, the problem with CNN loss functions, that learn the network to classify images (e.g. the SoftMax loss), is that CNNs are only able to identify those subjects which have been used for the training of the CNN. If new subjects are added to the biometric application system, then the CNN needs to be retrained or else a new subject can only be classified as one of the subjects that were used for CNN training (the one that is most similar to the newly added subject with respect to the CNN outputs). This makes the practical application of CNNs trained with such loss functions impossible for any biometric application including fish-eye recognition. The triplet loss does not learn the CNN to classify images, but to generate feature vectors from images in such a way that they are similar for images of identical classes and different for images of different classes. The triplet loss is applied to three training images (a so called triplet) at once, where two images belong to the same class (the so called Anchor image and a sample image from the same class, further denoted as Positive) and the third image belongs to a different class (further denoted as Negative). The triplet loss using the squared Euclidean distance is defined as follows:

$$L(A,P,N) = \max(\|f(A) - f(P)\|^2 \quad -\|f(A) - f(N)\|^2 + \alpha, 0), \quad (1)$$

where A is the Anchor, P the Positive and N the Negative. α is a margin that is enforced between positive and negative pairs and is set to $\alpha = 1$. $f(x)$ is an embedding (the CNN output) of an input image x. Fig. 3 shows the scheme of learning a CNN using the triplet loss. A triplet of training images (Anchor, Positive and Negative) is fed through the CNN resulting in an embedding for each of the three images. The embeddings of the three images are then used to

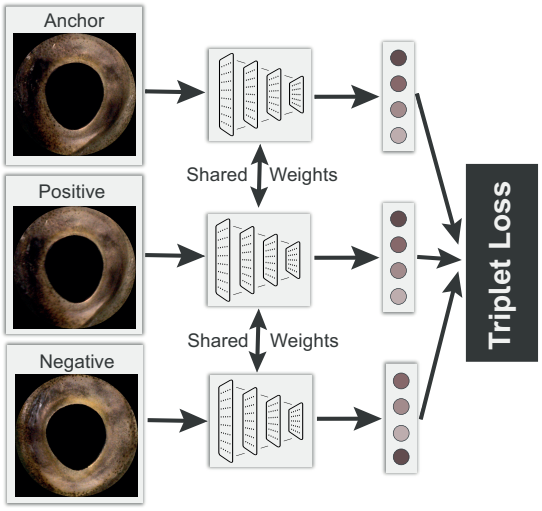

Figure 3: CNN training using the triplet loss

compute the triplet loss to update the CNN. Preliminary to CNN training, the iris images were first uniformly aligned using to the rotational pre-alignment vector Θ_0 and then cropped based on the approximated limbic boundary. It should be noted that the three iris images of a triplet can come from any LT or ST session. For fish iris recognition this means that the CNN is trained so that the Euclidean distances between the CNN outputs of all fish iris images of the same class (fish) is small (no matter in which LT sessions the images have been acquired), whereas the Euclidean distances between any pairs of CNN outputs from iris images of different fishes is large.

We employ hard triplet selection [14] for CNN training (only those triplets are chosen for training that actively contribute to improving the model). Iris images across all sessions (LT&ST) are used together for training so that the CNN may learn how fish eyes change during time and recognizes fish eyes even if they were acquired at different sessions. As CNN architecture we employ Squeeze-Net (SqNet) [15]. SqNet is a small neural network that is specifically created to have few parameters and only small memory requirements.

The size of the CNN's last layer convolutional filter is adapted so that a 256-dimensional output vector (embedding) is produced. To make the CNN more invariant to shifts in images and to increase the amount of training data, we employ data augmentation during CNN training. We apply random shifts in horizontal & vertical directions by first resizing the input images to a size of 234×234 and then extracting a patch of size 224×224 at a random position of the resized image (± 5 pixels in each direction). The CNN is trained for 400 epochs, starting with a learning rate of 0.001, which is divided by 10 every 120 epochs.

3 Experimental Setup

Basically, the experimental setup is different for the texture feature-based and the CNN-based experiments. The main focus is to make the results as comparable as possible.

For each DB and the texture feature-based and CNN-based approach results are computed with three configura-

tions: with MAX and PCA as rotational pre-alignment strategy and for one baseline configuration without rotational pre-alignment which is referred to as NO. For the texture feature-based approach for all fish iris images of a configuration in the LT&ST dataset of AS_{DB}&SB_{DB} feature vectors are computed. For each configuration and DB matching scores (MSs) are computed between all feature vector pair combinations. The MSs are computed using the Hamming distance and a shift value of 16 was used in order to compensate for remaining rotational variances.

For the CNN-based approach we employ a 2-fold cross validation for each DB. The CNN is trained twice for each DB, first using one fold for training and the other for evaluation, and then vice versa. Each fold consists of the images from half of the pre-processed fish iris images over all sessions of a configuration. That means the iris images of one fish (no matter in which session they were acquired) are all in the same fold. The configurations are the same as for the texture feature-based approach. We have to consider that each of the two trained CNNs per DB (one per fold) has a different mapping of the images to the CNN output feature space. Thus, feature vectors of different folds cannot be compared and therefore any performance metric has to be computed for each of the two folds separately using only MSs between images of the same fold. The MSs can be subdivided according to LT&ST datasets of each DB and for each configuration. MSs computed between feature vectors from the same session are denoted as session MSs and MSs computed between different sessions are referred to as temporal MSs. The score distribution (SD) computed for the session MSs from the ST dataset S1 together with the LT dataset S1 is is denoted as $S1_{all}$. Furthermore, session MSs are computed for the different sessions of the LT dataset which results in four different score distributions for AS_{DB} and two for SB_{DB} denoted S1,S2,S3 and S4 respectively. Temporal MSs are computed between the different sessions of the LT dataset which leads to six different comparisons for AS_{DB} (S1↔S2, S2↔S3, S3↔S4, S1↔S3, S2↔S4 and S1↔S4) and to one comparison for SB_{DB} (S1↔S2). For limiting computational costs, we have decided to present verification results in performance evaluation, i.e. we compute the Equal Error Rates (EERs). Also, the EER is well suited to compare the CNN-based results to the texture feature-based approaches. Although not suited for practical application, the accuracy of verification results does carry over to the accuracy of the multiple recognition stages in identification.

4 Results and Discussion

For the experimental evaluation different aspects are assessed. First, for AS_{DB} and SB_{DB} the CNN-based approach is compared to the texture feature-based approach. Second, distinctiveness and stability of the seabass iris are considered in detail and compared to the AS results and it is assessed if rotational pre-alignment works for the seabass iris and if it is required for the CNN-based approach. In regard to the stability of the fish iris it is interesting to see how the CNN-based approach performs compared to the texture feature-based approach.

Results for AS_{DB}&SB_{DB} are presented in Table 1 and 2, respectively. For the CNN-based results and each rotational pre-alignment configuration, the EERs computed for each fold, indicated by a subscript 0 or 1 in the abbreviation, and the averaged EERs are presented. For the AS_{DB} results in Table 2 the texture feature-based results computed in [7] are shown. The utilized configurations are the same as applied for the SB_{DB} texture feature-based approach as described in Sec. 3.

Basically, it can be said that the CNN-based results are significantly worse than the texture feature-based ones. Considering the LT results (AS_{DB}&SB_{DB}) it can be stated that the CNN-based approach does not improve the LT verification performances. Regarding the need or suitability of rotational pre-alignment in case of the CNN-based approach the results vary. For AS_{DB} which shows more rotational variances than SB_{DB} it can be concluded that rotational pre-alignment brings quite a bit of improvement, however, for some results rotational pre-alignment slightly decreases the EERs. When comparing the AS_{DB} LT CNN-based and texture feature-based results it is shown that the CNN-based approach is not as dependent on rotation compensation as the texture feature-based approach. The SB_{DB} results indicate a high distinctiveness of the seabass iris when looking at the texture-based results for $S1_{all}$. Same as for the salmon iris a low stability of the seabass iris is observed. Regarding rotational pre-alignment, PCA improves the CNN-based verification performances for SB_{DB}. For the texture feature-based results there is not much difference which can be attributed to rotational pre-alignment. It should be noted again that SB_{DB} involves less rotational variances and therefore the texture-based approach does not benefit from rotational pre-alignment as shown for the LT AS_{DB} results. However, results indicate that rotational pre-alignment works for the seabass iris because the EERs do not decrease in case of rotational pre-alignment, i.e. compare the EER for NO to the PCA and MAX EERs for the texture feature-based approach. Fig. 4 illustrates the intra-/interclass score distributions for $S1_{all}$, PCA, SB_{DB} for the CNN-based and the texture feature-based approach. In contrast to the CNN-based approach, the texture feature-based approach enables to separate the two distributions clearly.

5 Conclusions

Individual fish identification is required to establish continuous monitoring in intensive aquaculture in order to move towards precision farming. Previous research showed the feasibility of Atlantic salmon iris identification using a texture feature-based approach. Results showed a high distinctiveness but a low stability of the salmon iris.

Approach	ROT	ST/LT			
		$S1_{all}$	S1	S2	S1↔S2
CNN	NO_0	13.87	15.47	20.46	38.47
	NO_1	6.66	8.37	10.99	37.69
	NO	10.27	11.92	15.73	38.08
	PCA_0	5.40	7.82	15.71	34.8
	PCA_1	6.06	6.10	7.47	40.62
	PCA	5.73	6.96	11.59	37.71
	MAX_0	10.27	13.42	20.17	43.63
	MAX_1	7.06	8.45	16.36	32.91
	MAX	8.67	10.94	18.27	38.27
Texture	NO	0.27	0.00	1.04	25.40
	PCA	0.30	0.00	1.63	22.52
	MAX	0.54	0.00	2.49	23.60

Table 1: European seabass iris verification performances (EERs [%])

Approach	ROT	Session SDs (ST)					Temporal SDs (LT)					
		$S1_{all}$	S1	S2	S3	S4	S1↔S2	S2↔S3	S3↔S4	S1↔S3	S2↔S4	S1↔S4
CNN	NO_0	3.39	9.5	11.54	5.25	7.08	26.44	45.60	42.46	22.37	44.08	30.31
	NO_1	3.50	12.40	14.39	11.88	11.18	24.31	33.97	49.89	25.6	49.16	26.02
	NO	3.40	10.95	12.9	8.565	9.13	25.38	39.79	46.18	23.99	46.62	28.1
	PCA_0	5.70	10.46	17.43	19.02	19.11	28.89	48.58	40.48	34.24	43.19	33.05
	PCA_1	4.71	5.68	12.09	11.09	9.33	21.93	32.8	49.14	25.06	48.03	19.63
	PCA	5.21	8.07	14.76	15.06	14.22	25.41	40.69	44.81	29.65	45.61	26.34
	MAX_0	2.79	8.59	11.36	12.66	15.28	12.62	40.73	51.1	11.71	43.43	19.37
	MAX_1	4.58	4.59	13.68	11.41	14.24	16.58	42.61	47.92	20.28	43.96	17.35
	MAX	3.69	6.59	12.52	12.04	14.76	14.6	41.67	49.51	15.10	43.70	18.36
Texture	NO	0.65	0.71	2.52	0.15	3.91	47.02	36.94	42.74	39.14	46.16	49.37
	PCA	0.92	1.03	0.29	0.19	5.88	27.91	11.69	36.4	40.67	42.81	43.05
	MAX	3.94	0.45	0.21	0.06	15.02	15.52	10.32	28.35	15.42	29.28	37.84

Table 2: Atlantic salmon iris verification performances (EERs [%])

Lighter coloured values in Table 1 and Table 2 show the EERs computed for each fold of the CNN-based approach. Green coloured results signalize the lowest EERs computed for each ST/LT dataset.

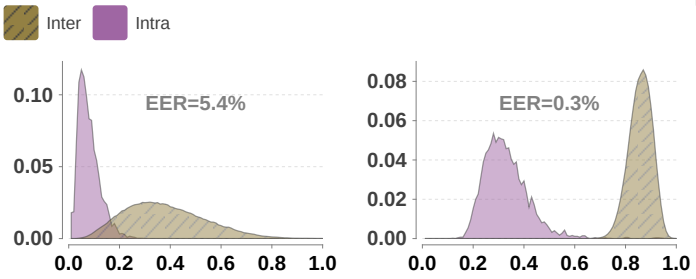

(a) CNN, PCA_0 (b) Texture feature-based, PCA

Figure 4: Intra-/Interclass distribution charts for SB_{DB}, $S1_all$ [X-Axis: Matching Score, Y-Axis: Probability]

Therefore, this work investigated if a CNN-based approach is suited to improve the long term stability. For this reason, the results for the salmon iris images were recomputed using a CNN-based approach and for a new DB with iris images from European seabass. Furthermore, rotational pre-alignment was applied to assess if it is required for the CNN-based approach and if it is applicable to the seabass iris. For seabass additionally results using the texture feature-based approach were computed. This enabled to assess if iris recognition is applicable to another fish species and if the basic statements are the same as for the salmon iris.

Same as for salmon, results indicate a high distinctiveness of the seabass iris but it shows a low long term stability. Interestingly, the CNN-based approach performs worse compared to the texture feature-based approach. Regarding rotational pre-aligment it can be stated that it is required for the texture feature-based approach. For the CNN-based approach the improvement due to rotational pre-alignment is not that significant. The lower recognition accuracy of the CNN-based approach might be attributed to the relatively small amount of data. Therefore, we will refine the evaluation by looking at k-fold cross validation results with increasing k (which requires increasing training effort of course). Future work needs to deal with iris images captured in a realistic environment.

Acknowledgements

Supported by the Ministry of Education, Youth and Sports of the Czech Republic – project CENAKVA (LM2018099), AQUAEXCEL2020 projects (652831,AE050006) and GAJU 013/2019/Z.

References

[1] J. P. Barriga, J. M. Chiarello-Sosa, R. Juncos, and M. Á. Battini, "Photo-identification and the effects of tagging on the patagonian catfish hatcheria macraei," Environmental Biology of Fishes, vol. 98, no. 4, 2014 (cit. on p. 2).

[2] L. H. Stien et al., "Consistent melanophore spot patterns allow long-term individual recognition of atlantic salmon salmo salar," Journal of Fish Biology, vol. 91, no. 6, 2017 (cit. on p. 2).

[3] L. C. T. Chaves, J. Hall, J. L. L. Feitosa, and I. M. Côté, "Photo-identification as a simple tool for studying invasive lionfish populations," Journal of Fish Biology, vol. 88, no. 2, 2015 (cit. on p. 2).

[4] J. Merz, P. Skvorc, S. Sogard, C. Watry, S. Blankenship, and E. V. Nieuwenhuyse, "Onset of melanophore patterns in the head region of chinook salmon: A natural marker for the reidentification of individual fish," North American Journal of Fisheries Management, vol. 32, no. 4, 2012 (cit. on p. 2).

[5] G. Castillo et al., "Using natural marks to identify individual cultured adult delta smelt," North American Journal of Fisheries Management, vol. 38, no. 3, 2018 (cit. on p. 2).

[6] R. Dala-Corte, J. Moschetta, and F. Becker, "Photo-identification as a technique for recognition of individual fish: a test with the freshwater armored catfish," Neotropical Ichthyology, vol. 14, 2016, issn: 1679-6225 (cit. on p. 2).

[7] R. Schraml et al., “Towards fish individuality-based aquaculture,” IEEE Transactions on Industrial Informatics, vol. 17, no. 6, 2021 (cit. on pp. 2–5).

[8] P. Cisar, D. Bekkozhayeva, O. Movchan, M. Saberioon, and R. Schraml, “Computer vision based individual fish identification using skin dot pattern,” Scientific Reports, vol. 11, no. 1, 2021 (cit. on pp. 2, 3).

[9] K. Sundararajan and D. L. Woodard, “Deep learning for biometrics: A survey,” vol. 51, no. 3, 2018, issn: 0360-0300 (cit. on pp. 2, 4).

[10] J. Daugman, “The importance of being random: Statistical principles of iris recognition,” Pattern Recognition, vol. 36, no. 2, 2003 (cit. on p. 4).

[11] L. Masek, “Recognition of human iris patterns for biometric identification,” M.S. thesis, University of Western Australia, 2003 (cit. on p. 4).

[12] University of Salzburg, USIT – University of Salzburg iris toolkit, http://www.wavelab.at/sources/USIT, University of Salzburg, 2017 (cit. on p. 4).

[13] Z. Zhao and A. Kumar, “Towards more accurate iris recognition using deeply learned spatially corresponding features,” in 2017 IEEE International Conference on Computer Vision (ICCV), 2017 (cit. on p. 4).

[14] F. Schroff, D. Kalenichenko, and J. Philbin, “Facenet: A unified embedding for face recognition and clustering,” in 2015 IEEE Conference on Computer Vision and Pattern Recognition (CVPR), 2015 (cit. on p. 4).

[15] F. N. Iandola, M. W. Moskewicz, K. Ashraf, S. Han, W. J. Dally, and K. Keutzer, “Squeezenet: Alexnet-level accuracy with 50x fewer parameters and <1mb model size,” CoRR, vol. abs/1602.07360, 2016. arXiv: 1602.07360 (cit. on p. 4).